Identification of GDP as a small inhibitory molecule in HepG2 cells by non-targeted metabolomics analysis

ZHILIN PENG[1,2*], SITING XU[1,2*], HAOCHENG WANG[1,2], YANLI HUANG[1,2], SIYUAN LIU[1,2], ZHONGBEI JIAO[1,2], MEI LIN[1,2], PING ZHU[3], YU CHEN[3], YAN SHI[3], YUEQUN WANG[1,2], YONGQING LI[1,2], WUZHOU YUAN[1,2], XIUSHAN WU[1,2], ZHIGANG JIANG[1], FANG LI[1] and XIONGWEI FAN[1,2]

[1]The Center for Heart Development, College of Life Science, Hunan Normal University, Changsha, Hunan 410081, P.R. China; [2]State Key Laboratory of Developmental Biology of Freshwater Fish, College of Life Sciences, Hunan Normal University, Changsha, Hunan 410081, P.R. China; [3]Guangdong Provincial Key Laboratory of Pathogenesis, Targeted Prevention and Treatment of Heart Disease, Guangdong Provincial People's Hospital Affiliated to Southern Medical University, Guangzhou, Guangdong 510100, P.R. China

Received July 22, 2024; Accepted December 12, 2024

DOI: 10.3892/ol.2025.14924

Abstract. Identifying the mechanism by which lipid metabolism regulates cancer may offer a novel approach for therapeutic intervention. It has previously been identified that a lipid metabolism-related factor, namely fatty acid hydroxylase domain containing 2 (FAXDC2), is downregulated in various types of cancer, and inhibits the proliferation and migration of liver cancer cells through a mechanism associated with ERK. The liver is important for lipid metabolism, and FAXDC2 is involved in the synthesis of cholesterol and sphingomyelin. However, the functional mechanism by which FAXDC2 influences liver cancer cells through metabolic processes and ERK signaling remains unclear. Therefore, the present study induced the overexpression of FAXDC2 in HepG2 liver cancer cells and performed a metabolomics analysis. This identified guanosine diphosphate (GDP) as a significantly altered metabolite. Using AlphaFold3, a robust interaction was predicted between FAXDC2 and GDP, which lead to the hypothesis that GDP may mediate the inhibitory effects of FAXDC2 on liver cancer cells by directly modulating the functional properties of the cells, thereby influencing their behavior and progression. Cell Counting Kit-8 assays were used to study the impact of elevated GDP concentrations on HepG2 cell growth. The results revealed a gradual reduction in the viability of HepG2 cells as the GDP concentration increased. In addition, western blotting showed that GDP treatment was accompanied by a significant downregulation of cyclin dependent kinase 4 and cyclin D1 expression levels, and Transwell experiments revealed that GDP treatment significantly decreased the invasion of HepG2 cells. Treatment with GDP also significantly inhibited the expression of ERK. In summary, the present study is the first to indicate that GDP is a metabolic small molecule with inhibitory activity in cancer cells, which has previously been overlooked in tumor metabolic reprogramming. The study findings offer new insights and strategies for the diagnosis and treatment of liver cancer, and potentially other types of cancer.

Correspondence to: Professor Xiongwei Fan, The Center for Heart Development, College of Life Science, Hunan Normal University, 177 Lushan Road, Yuelu, Changsha, Hunan 410081, P.R. China
E-mail: 16119@hunnu.edu.cn

*Contributed equally

Key words: lipid metabolism, fatty acid hydroxylase domain containing 2, liver cancer, metabolomics, ERK, guanosine diphosphate, AlphaFold3

Introduction

Liver cancer is one of the most frequently diagnosed types of cancer worldwide and a leading cause of cancer-associated mortality (1-6). It is estimated that, by 2025, the number of cases of liver cancer worldwide will be >1 million (7). Presently, this category of malignant disease imposes an escalating burden on individuals, families and societies; notably, it incurs substantial economic costs and introduces elements of instability. Therefore, it is particularly important to elucidate the pathogenic mechanism underlying liver cancer as this should facilitate the development of effective strategies for the prevention and control of this disease.

In order to maintain their rapid proliferation, cancer cells rely on a continuous supply of energy and materials. Therefore, compared with normal healthy cells, cancer cells exhibit alterations in the metabolism of matter and energy, including changes in glucose, lipid and protein metabolism. Proliferation is a core behavior of all cancer cells; this encompasses the pivotal involvement of fatty acids in the synthesis of biomembranes, as well as the engagement of signaling molecules, thereby underscoring the association of the reprogramming of lipid metabolism with the pathogenesis and progression of cancer (8-11). The liver is the core organ that maintains fat metabolism and homeostasis. The reprogramming of liver lipid metabolism during the development of liver cancer is

a topic of interest to researchers. It has been shown that in the transformation of non-alcoholic steatohepatitis into liver cancer, the activation of a variety of oncogenic signals and fatty acid metabolism signals occurs, and targeted inhibition of the lipoprotein lipase/fatty acid-binding protein 4/carnitine palmitoyltransferase 1 fatty acid metabolism signaling axis can prevent this transformation; this indicates that the activation of signaling pathways associated with fatty acid metabolism may be involved in the initiation and maintenance of hepatocellular carcinogenesis (12). Mitochondria are important sites for lipolysis and anabolism. Mitochondrial fission facilitates the shift in glucose metabolism from glycolysis to oxidative phosphorylation, thereby alleviating the energy stress associated with tumor survival (13). In addition, mitochondrial fission promotes fatty acid synthesis in liver cancer cells, inhibits fatty acid oxidation and regulates the reprogramming of lipid metabolism to promote liver cancer cell proliferation, metastasis and tumor growth *in vivo* (13). The upregulation of fatty acid and cholesterol synthesis, and changes in fatty acid oxidation are key features of fatty acid metabolism reprogramming in cancer cells (14,15). Signaling molecules that regulate fatty acid and cholesterol metabolism are undergoing evaluation as new therapeutic targets for liver cancer (16). Although it has been shown that lipid metabolism reprogramming plays an important role in the occurrence and development of liver cancer, the specific molecular mechanisms are not yet fully understood.

The mitogen-activated protein kinase (MAPK)/extracellular signal-regulated kinase (ERK) signaling pathway is a key pathway that regulates a variety of cellular processes, including cell proliferation, differentiation, migration and aging (17). The MAPK/ERK signaling pathway is activated through signal transduction via cell surface receptors (18). Dysregulation of this pathway can lead to cell abnormalities, which are manifested as an excessive increase in cell growth and proliferation, dedifferentiation and enhanced survival ability; these abnormalities jointly promote the occurrence of cancer (18). There are a number of specific receptor tyrosine kinases that can trigger this pathway, including platelet-derived growth factor receptor, epidermal growth factor receptor (EGFR), fibroblast growth factor receptor and vascular endothelial growth factor receptor (19). However, the mechanism by which the regulation of lipid metabolism affects the MAPK/ERK signaling pathway has not yet been clearly interpreted.

Fatty acid hydroxylase domain containing 2 (FAXDC2), also known as C5orf4, is a member of the fatty acid hydroxylase superfamily. It has been reported that the expression of FAXDC2 is downregulated in prostate cancer and neuroblastoma, and that the low expression of FAXDC2 is an unfavorable factor for the prognosis of these diseases (20,21). In addition, it has been shown that FAXDC2 regulates megakaryocyte differentiation through mechanisms associated with the regulation of ERK signaling (22). Our previous study (23) demonstrated that the expression of FAXDC2 is downregulated in various types of cancer, including liver cancer, and its low expression is significantly associated with a poor prognosis. In addition, it revealed that the overexpression of FAXDC2 inhibited the proliferation and invasion of HepG2 cells. Given that the liver is important for lipid metabolism and FAXDC2 is a hydroxylase involved in cholesterol and sphingomyelin synthesis, the overexpression of which can inhibit ERK phosphorylation, it was hypothesized that FAXDC2 may mediate its tumor-suppressive effects via the inhibition of ERK phosphorylation.

Despite interest in the association between metabolism and cancer, studies directly assessing the relationship between metabolic small molecules and tumor metabolism remain limited. The present study employed high-throughput metabolomics analysis to investigate the mechanisms by which FAXDC2 modulates the proliferation and invasion of liver cancer cells through cellular metabolism. Since this identified a significant increase in guanosine diphosphate (GDP) levels in HepG2 cells following FAXDC2 overexpression, the present study also examined the comprehensive expression profiles of liver cancer cells following FAXDC2 overexpression and concomitant GDP elevation and delineated their inhibitory effects on the proliferation and invasion of liver cancer cells.

Materials and methods

Cell culture, FAXDC2 overexpression and GDP treatment. HepG2 cells (cat. no. HB-8065; American Type Culture Collection) were cultured in Dulbecco's modified Eagle's medium (Gibco; Thermo Fisher Scientific, Inc.) containing 10% fetal calf serum [Serana (WA) Pty, Ltd.], 100 U/ml penicillin and 100 μg/ml streptomycin (cat. no. C0222; Beyotime Institute of Biotechnology). Transfection of HepG2 cells was performed using Lipofectamine® 2000 (Invitrogen; Thermo Fisher Scientific, Inc.) according to the manufacturer's protocol. Cells were transfected at ~80% confluence, with 5 μg plasmid/dish, The plasmid was incubated with Lipofectamine for 10 min, then the DNA-lipid complex was added to the cells and incubated for 48 h at 37˚C. FAXDC2 overexpression was achieved by inserting the coding sequence of human FAXDC2 (Accession no. NM_032385) into the pCMV-HA vector (Agilent Technologies, Inc.) to generate pCMV-HA-FAXDC2. Empty pCMV-HA vector was used as a negative control for overexpression. GDP was diluted with medium before being used to treat the cells for 48 h. The GDP concentrations were 20, 40, 80, 160 and 200 μM. The cells were treated and cultured at 37˚C and 5% CO_2.

Reverse transcription-quantitative PCR (RT-qPCR). Total RNA was extracted from cells utilizing the FastPure Complex Tissue/Cell Total RNA Isolation Kit (cat. no. RC113-01; Vazyme Biotech Co., Ltd.), according to the manufacturer's protocol. Subsequently, cDNA synthesis was achieved by employing the HiScript II 1st Strand cDNA Synthesis Kit (+gDNA wiper) (cat. no. R212-01; Vazyme Biotech Co., Ltd.), again according to the manufacturer's guidelines. qPCR was performed using SYBR Premix Ex Taq II (Takara Bio, Inc.), according to the manufacturer's protocol. The qPCR cycling conditions were as follows: Initial denaturation at 50˚C for 2 min; followed by a second denaturation at 95˚C for 5 min; and then 40 cycles of amplification, each consisting of denaturation at 95˚C for 15 sec and annealing/extension at 60˚C for 40 sec. The primers employed in the PCR analysis were sourced from TsingKe Biological Technology. For quantification purposes, the expression levels of GAPDH served as an internal reference, and the relative expression levels of

FAXDC2 were determined using the $2^{-\Delta\Delta Cq}$ method (24). The primer sequences were as follows: FAXDC2 forward, 5'-GGC TGCTGACTACATTTGAAGG-3' and reverse, 5'-TCAACC ACCAATAGAAGCCCA-3'; GAPDH forward, 5'-TGCACC ACCAACTGCTTAGC-3' and reverse 5'-GGCATGGACTGT GGTCATGAG-3'. Each RT-qPCR analysis was repeated three times.

Untargeted metabolomics analysis. The culture medium was removed from the HepG2 cells transfected with FAXDC2 overexpression vector or empty vector, and the plate was washed 2 or 3 times with pre-cooled PBS. Subsequently, the supernatant was discarded, trypsin was added for digestion and the cells were washed a further 2 or 3 times with PBS. The cells were then transferred to a centrifuge tube at 4˚C and were centrifuged at 4˚C, 1,200 x g for 2 min, after which the supernatant was discarded, and the cells were collected and placed into a 1.5-ml microcentrifuge tube. The cells were frozen in liquid nitrogen for 15 min and then prepared for analysis by liquid chromatography-mass spectrometry (LC-MS). The LC-MS detection and subsequent steps were all performed by Novogene Co. Ltd.

Bioinformatics. Raw data from the LC-MS analysis underwent preprocessing with the Compound Discoverer 3.3 data processing software (https://www.thermofisher.cn/order/catalog/product/OPTON-31056), followed by metabolite identification through alignment with high-resolution tandem mass spectrometry databases including mzCloud (beta.mzcloud.org), mzVault and the MassList primary database (both Thermo Fisher Scientific, Inc.). Using the relative quantitative values of the metabolites, Pearson correlation coefficients were computed among quality control samples (25). Partial least squares discrimination analysis was then applied, utilizing partial least squares regression (26) to model the relationships between metabolite expression levels and sample categories, enabling the classification and prediction of sample types. Principal component analysis was performed with the logarithmic transformation and standardization of data using MetaX (version: 1.4.17) (27). Furthermore, Kyoto Encyclopedia of Genes and Genomes (KEGG) pathway analysis was conducted using the KEGG database (https://www.genome.jp/kegg/pathway.html), with categorization of the biological metabolic pathways into the seven primary KEGG groups: Metabolism, Genetic Information Processing, Environmental Information Processing, Cellular Processes, Organismal Systems, Human Diseases and Drug Development. The Human Metabolome Database (HMDB; https://hmdb.ca/metabolites) was employed to elucidate the biological roles, disease associations, chemical reactions, metabolic pathways and other pertinent details of human metabolites.

AlphaFold3. The AlphaFold3 server (28) (https://www.alphafoldserver.com) was used to predict if there is likely to be any interaction between GDP and FAXDC2.

ELISA for the detection of intracellular GDP. The human GDP content detection ELISA kit was purchased from Tianjin Ruichuang Biotechnology Co., Ltd. (cat. no. RC-E110643A). The culture medium was removed from cultured cells, and the cells were washed with PBS and then treated with cell lysis solution. After centrifugation at 4˚C, 16,260 x g for 5 min, ELISA of the supernatant was performed. Briefly, standard and sample wells were set up, then horseradish peroxidase (HRP)-labeled detection antibodies were added to the wells and incubated in a water bath at 37˚C for 60 min. The liquid was then discarded and the wells were washed five times with washing solution. After allowing to stand for 1 min, Substrates A and B were added, the wells were incubated at 37˚C in the dark for 15 min, and then stop solution was added. The optical density (OD) of each well was measured using a microplate reader, and the GDP content of the sample was calculated from a standard curve.

Cell Counting Kit-8 (CCK-8) assay. Cell viability was assessed using the CCK-8 assay (Beyotime Institute of Biotechnology). At 24, 48 and 72 h after GDP treatment, 20 μl CCK-8 reagent was added to each well, and the cells were incubated in a humidified CO_2 incubator at 37˚C for 1 h. The OD of the culture medium was then measured as the absorbance at a wavelength of 450 nm using a microplate reader (Bio-Rad Laboratories, Inc.).

Transwell assay. Cell invasion assays were performed in 24-well plates with a 8-μm chamber insert in each well (Corning, Inc.). To evaluate invasion, Matrigel was defrosted at 4˚C and layered on an insertion membrane to form a matrix barrier. The membrane was then placed in a 37˚C incubator for 30 min to solidify, and $1x10^5$ cells were seeded in the upper chamber after suspension in serum-free medium. Then, 800 μl medium containing 10% FBS was added to the lower chamber and the chamber was carefully placed into a 24-well plate and cultured in an incubator at 37˚C for 48 h. Cells that adhered to the underlying membrane were fixed and stained using a mixture of 0.1% crystal violet and 20% methanol for 30 min at room temperature. Images of the cells were then captured and the cells were counted under an inverted microscope (Nikon Eclipse; Nikon Corporation). Each experimental group consisted of three biological replicates.

Western blotting. Total cellular proteins were extracted from cells with RIPA lysis buffer (Wuhan Elabscience Biotechnology Co., Ltd.), and protein concentrations were quantified using the BCA assay. Proteins (20 μg protein/lane) were then loaded onto 10% polyacrylamide gels and electrophoresis was performed at a constant voltage of 100 V to separate the protein bands. Protein transfer was performed at a constant current of 300 mA; transfer was to a PVDF membrane that had been activated with methanol for 30 sec before use. Subsequently, the PVDF membrane was blocked by soaking in 5% skimmed milk in Tris-buffered saline-0.05% Tween 20 (TBST) for 1.5 h at room temperature and the excess milk was washed away with TBST. The PVDF membrane was then incubated with primary antibodies (1:1,000 dilution) for 90 min at room temperature and washed three times with TBST (5 min/wash). Subsequently, the PVDF membrane was incubated at room temperature for 90 min with the secondary antibody (1:5,000 dilution) and then washed three times with TBST (5 min/wash). Super-sensitive ECL chemoluminescent substrate (cat. no. BL520A; Biosharp Life Sciences) was used

for film imaging. Semi-quantitative analysis was performed using ImageJ 1.52a software (http://imagej.org; National Institutes of Health). Anti-phosphorylated-p44/42 MAPK (ERK1/2) (cat. no. 4370), anti-p44/42 MAPK (ERK1/2) (cat. no. 4695) and anti-cyclin-dependent kinase 4 (CDK4; 12790) were purchased from Cell Signaling Technology, Inc.; anti-c-Myc protein (cat. no. TA0358), anti-EGFR (cat. no. T55112), anti-cyclin D1 protein (cat. no. TC52046) and anti-tubulin protein (cat. no. M30109) antibodies were purchased from Abmart (Shanghai) Co., Ltd. HRP-conjugated goat anti-mouse IgG and anti-rabbit IgG secondary antibodies were purchased from CoWin Biosciences (1:5,000; cat. nos. CW0102 and CW0103).

Statistical analysis. Statistical analysis was performed using GraphPad Prism 8.0 software (GraphPad; Dotmatics). Data are presented as the mean ± standard deviation. The data of the GDP experiment were verified to conform to a normal distribution. Differences between two groups were evaluated using unpaired Student's t-test. CCK-8 assay data were analyzed by one-way ANOVA followed by Dunnett's post hoc tests. $P<0.05$ was considered to indicate a statistically significant difference.

Results

Enrichment classification of differential metabolites detected using untargeted metabolomics analysis. Our previous study showed that FAXDC2 inhibits the proliferation and invasion of HepG2 cells (23). To elucidate the regulatory mechanisms of FAXDC2 in lipid metabolism and substance synthesis, given its classification as a member of the fatty acid hydroxylase superfamily, it was hypothesized that perturbations in the expression of FAXDC2 could potentially modulate the metabolic landscape of HepG2 cells, a widely used cell line in hepatic metabolism research. Consequently, a comprehensive, non-targeted metabolomics analysis was performed, in which the metabolic profiles of HepG2 cells subjected to overexpression of FAXDC2 were compared with those of HepG2 cells transfected with an empty vector control. This approach aimed to identify specific metabolic alterations that may be attributed to the modulation of FAXDC2 expression levels. To validate the experimental paradigm, RT-qPCR analysis was initially conducted on HepG2 cells subjected to overexpression of FAXDC2 in comparison with those subjected to transfection with empty vector control. The analysis confirmed the successful overexpression of FAXDC2 (Fig. 1A). In addition, a principal component analysis was performed, which identified a statistically significant disparity in the vector direction of the principal components between the experimental and control groups (Fig. 1B), indicative of distinct metabolic profiles between the two cohorts. Through the enrichment and annotation of differential metabolites in the HMDB, it was revealed that 'lipids and lipid-like molecules' were most enriched after the overexpression of FAXDC2 (Fig. 1C), which is consistent with the biological characteristics of FAXDC2. Through KEGG pathway enrichment analysis, it was observed that the differential metabolites detected after the overexpression of FAXDC2 were mainly enriched in pathways associated with metabolism (Fig. 1D), which indicated that the differential expression of FAXDC2 induces changes in metabolism-related pathways in HepG2 cells. Subsequently, a primary HMDB classification of the differential metabolites in HepG2 cells following the overexpression of FAXDC2 was performed. This revealed that the most prevalent category of these metabolites was 'lipids and lipid-like molecules' (Fig. 1E). This aligns well with the established biological function of FAXDC2 in lipid metabolism and biosynthesis.

Detection of differential metabolites based on untargeted metabolomics analysis. The correlations among differential metabolites in the FAXDC2-overexpressing cells and their interactions within the metabolic network were investigated. The top 20 ranked differential metabolites are displayed from smallest to largest significance level (P-value) in Fig. 2A. It was observed that GDP was positively correlated with malic acid, uridine diphosphate (UDP) and uridine 5'-diphosphoglucuronic acid (UDPGA), and negatively correlated with other differential metabolites. The relationships between these metabolites are visually represented by a chord diagram (Fig. 2B). The commonalities or similar properties of the three positively correlated metabolites primarily lies in their roles in cellular metabolism. They serve as crucial metabolic intermediates participating in various biochemical pathways, particularly those associated with energy production, synthesis and conversion processes (29,30). Subsequently, a z-score plot was constructed, which revealed that thymidine 5'-diphosphate, malic acid, daidzein, D-glucarate, UDP and its derivative UDPGA exhibited significantly increased levels in the FAXDC2-overexpressing cells compared with those in the control group transfected with empty vector (Fig. 3A).

Further analysis was conducted on the differential metabolites after FAXDC2 overexpression based on their changes in abundance, as depicted in a volcano plot (Fig. 3B). The metabolomics analysis revealed that 527 differential metabolites were collectively enriched, among which 71 exhibited significantly increased or decreased abundance. The 71 differential metabolites are illustrated in a heatmap (Fig. 3C).

A volcano plot of differential metabolites was generated by comparing the contribution values of differential metabolites between the FAXDC2 overexpression group and the empty vector control group. Variable importance in projection (VIP) values were calculated, which estimate the contribution or importance of metabolites in the model (Fig. 3D). The top three differential metabolites with increased abundance were pantetheine, thymidine 5'-diphosphate and GDP, with GDP having the highest VIP value. These findings indicate that the differential metabolite GDP may provide the greatest contribution to the differences between the FAXDC2 overexpression group and the empty vector control group.

Overexpression of FAXDC2 leads to increased GDP content in HepG2 cells. Several differential metabolites identified in the untargeted metabolomics analysis were screened. These included GDP, daidzein and 2-deoxyglucose-6-phosphate, with a focus on changes in GDP levels. GDP plays an important role in cellular energy metabolism and signal transduction. GTP is a key energy transfer molecule, similar to ATP, which provides energy for various biochemical reactions, including fatty acid synthesis and degradation. In certain critical enzyme-catalyzed reactions, GDP is converted to guanosine triphosphate (GTP), a process often accompanied by the release or absorption of energy (31).

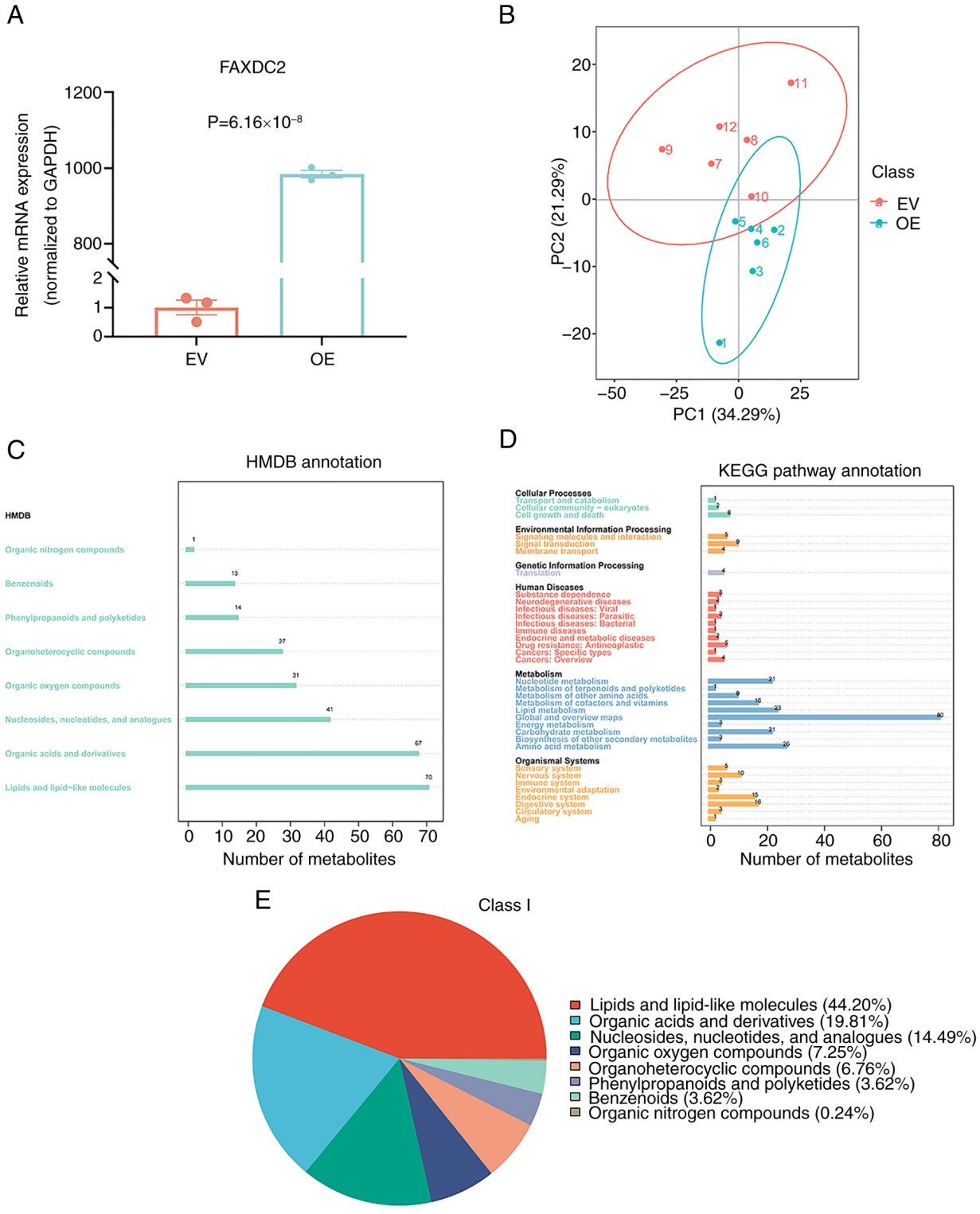

Figure 1. Differential metabolite classification in HepG2 cells after the overexpression of FAXDC2 assessed based on untargeted metabolomics. (A) Overexpression of FAXDC2 was confirmed by reverse transcription-quantitative PCR. Each set of experiments had three biological replicates. (B) Two-dimensional scatter plot of principal component analysis between the FAXDC2 overexpression and control groups. The abscissa represents the PC1 score, the ordinate represents the PC2 score, and the magnitude of the score determines its position along the PC1 or PC2 axis. (C) HMDB enrichment and annotation of differential metabolites. (D) KEGG pathway enrichment set analysis; the labels on the left are specific pathway names, and the numbers in the graph represent the differential metabolites enriched in the pathway. (E) First-level classification pie chart of differential metabolites, showing the proportions of different types of metabolites. FAXDC2, fatty acid hydroxylase domain containing 2; EV, empty vector; OE, overexpression; PC1/2, principal component 1/2; HMDB, Human Metabolome Database; KEGG, Kyoto Encyclopedia of Genes and Genomes.

In HepG2 cells overexpressing FAXDC2, the GDP levels were found to be higher than those in cells transfected with empty vector (Fig. 4A). Additionally, KEGG pathway enrichment analysis revealed that the differential metabolites were most enriched in the 'purine metabolism' pathway. It was also noted that GDP was the only differential metabolite

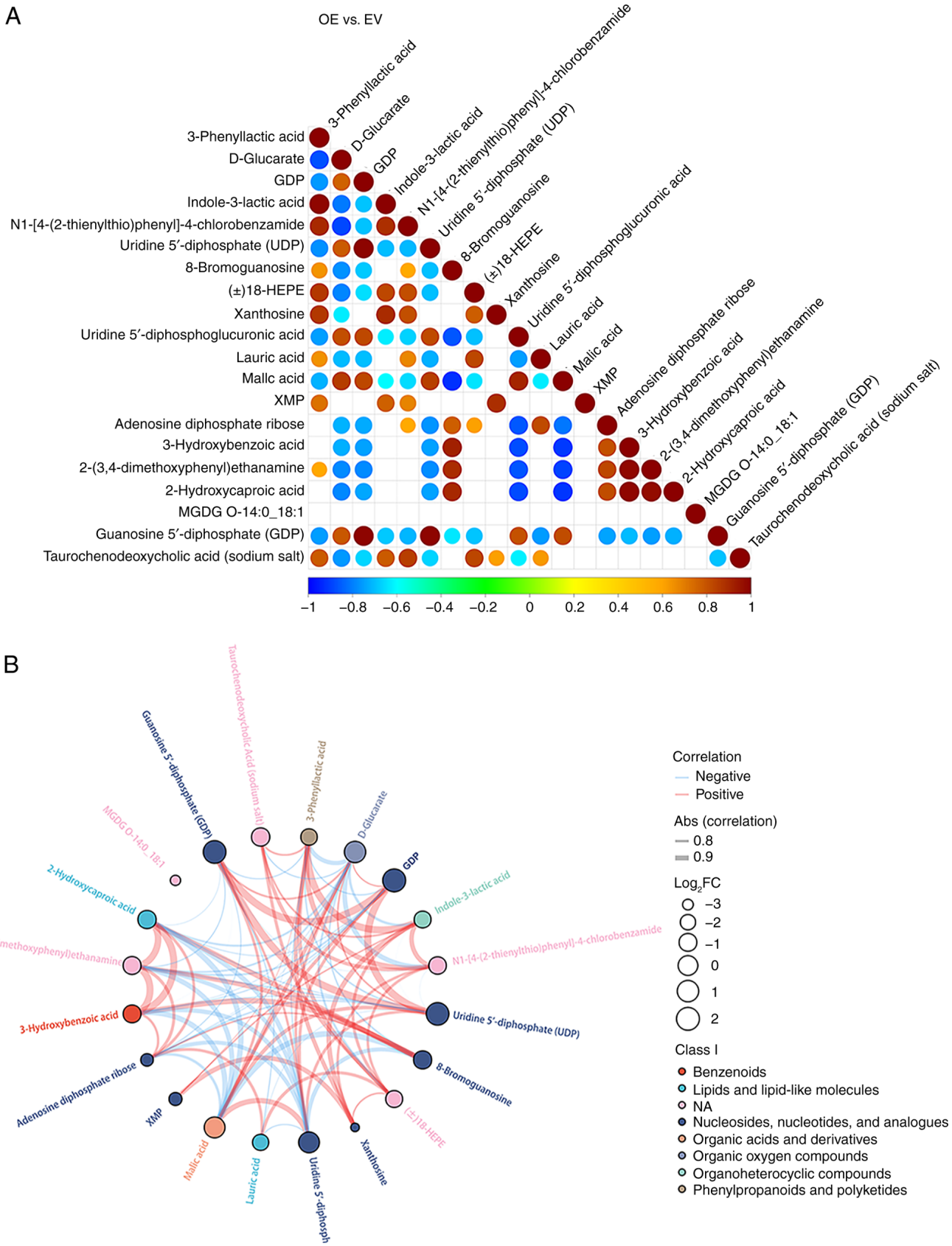

Figure 2. Correlation analysis of the differential metabolites of HepG2 cells after FAXDC2 overexpression detected by non-targeted metabolomics. (A) Correlation analysis plot of differential metabolites for the experimental group with overexpression of FAXDC2 compared with the control group. The top 20 differential metabolites from smallest to largest P-value are presented. The plot displays the Pearson correlation coefficients between each pair of differential metabolites. (B) Chord diagram of the top 20 differential metabolites providing a visual representation of the correlations among these metabolites. Blue represents a negative correlation, red represents a positive correlation, and blank represents no significant correlation. FAXDC2, fatty acid hydroxylase domain containing 2; OE, overexpression; EV, empty vector; GDP, guanosine diphosphate; 18-HEPE, 18-hydroxyeicosapentaenoic acid; XMP, xanthosine monophosphate; MGDG, monogalactosyldiacyl glycerol; Abs (correlation), absolute value of the correlation coefficient; log_2FC, log_2 fold change; NA, not available.

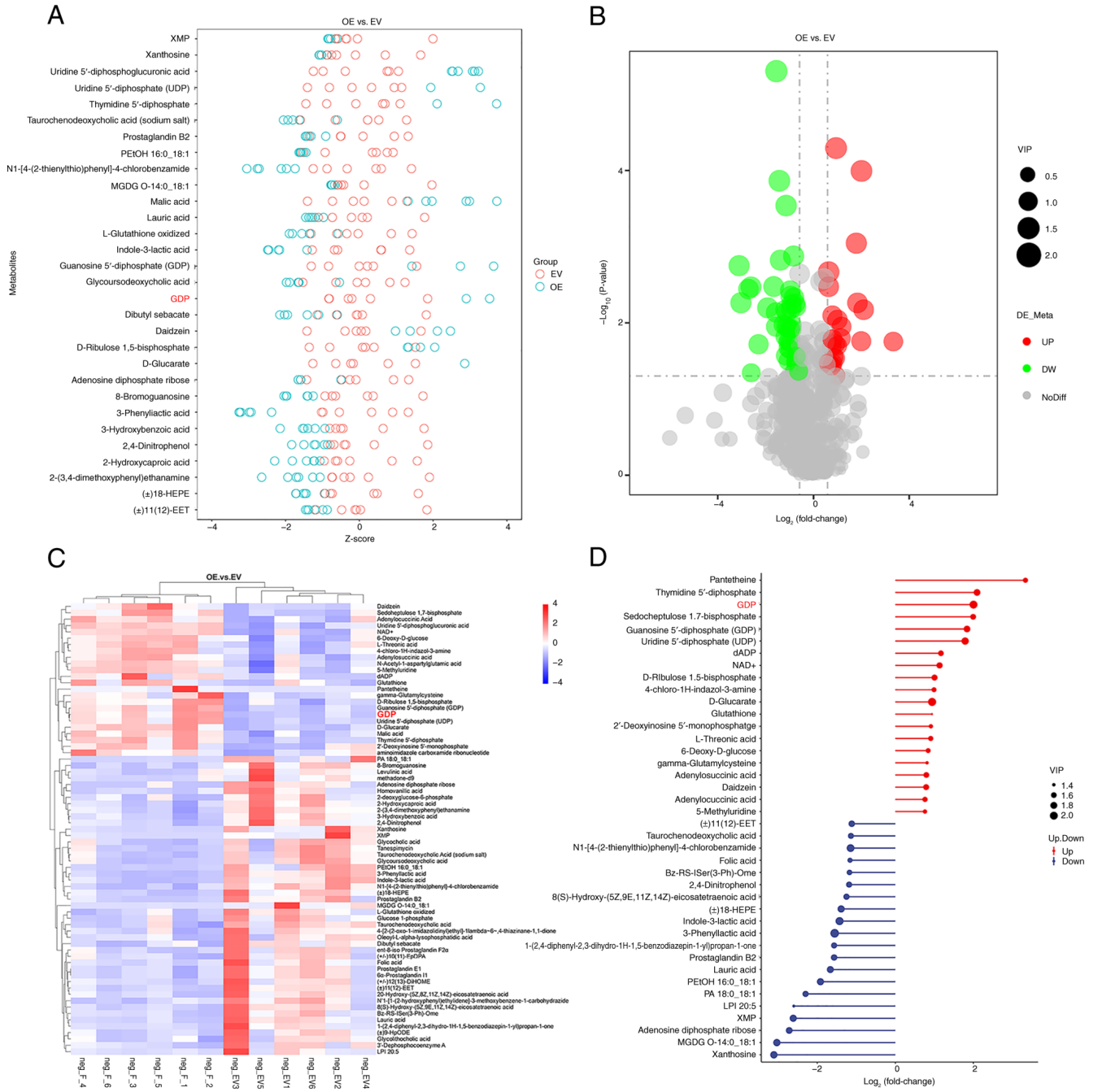

Figure 3. Differential metabolite differential analysis of HepG2 cells after the overexpression of FAXDC2 detected by non-targeted metabolomics. (A) Z-score plot representing the relative abundance of differential metabolites. Each circle represents a specific sample. The z-scores of the top 30 metabolites sorted by P-value from smallest to largest are displayed; samples with z-scores >4 or <-4 are not shown. (B) Volcano plot of differential metabolites. Green represents decreased abundance, red represents increased abundance, and gray represents no significant difference. (C) Heatmap of differential metabolites obtained by hierarchical clustering analysis performed on differential metabolites to reveal differences in metabolic expression patterns between and within groups. Upregulated differential metabolites are shown in red, while downregulated ones are shown in blue. (D) Matchstick plot of differential metabolites. The VIP values indicate the contribution of different differential metabolites to the difference between the FAXDC2 overexpression and empty vector control groups, where a higher value signifies greater contribution and importance. The circle size represents the VIP values, and the matchstick length represents the magnitude of the difference. Red represents increased abundance, while blue represents decreased abundance. FAXDC2, fatty acid hydroxylase domain containing 2; OE, overexpression; EV, empty vector; VIP, variable importance in projection; GDP, guanosine diphosphate; DE_Meta, differential expression meta-analysis; DW, down; NoDiff, no difference.

enriched in ‘Ras signaling pathway’ and ‘Rap1 signaling pathway’ (Fig. 4B).

A KEGG regulatory network diagram of the differential metabolites was then generated (Fig. 4C), which indicated a particular focus on GDP. Therefore, a KEGG regulatory network diagram specific for GDP was generated (Fig. 4D). It can be observed that GDP, as an input or known compound, may regulate the Ras signaling pathway. Since Ras is a crucial component of the MAPK/ERK signaling transduction pathway, changes in Ras may impact this pathway. This demonstrates the regulatory effect of FAXDC2 on the MAPK/ERK signaling transduction pathway, consistent with our previous study (23).

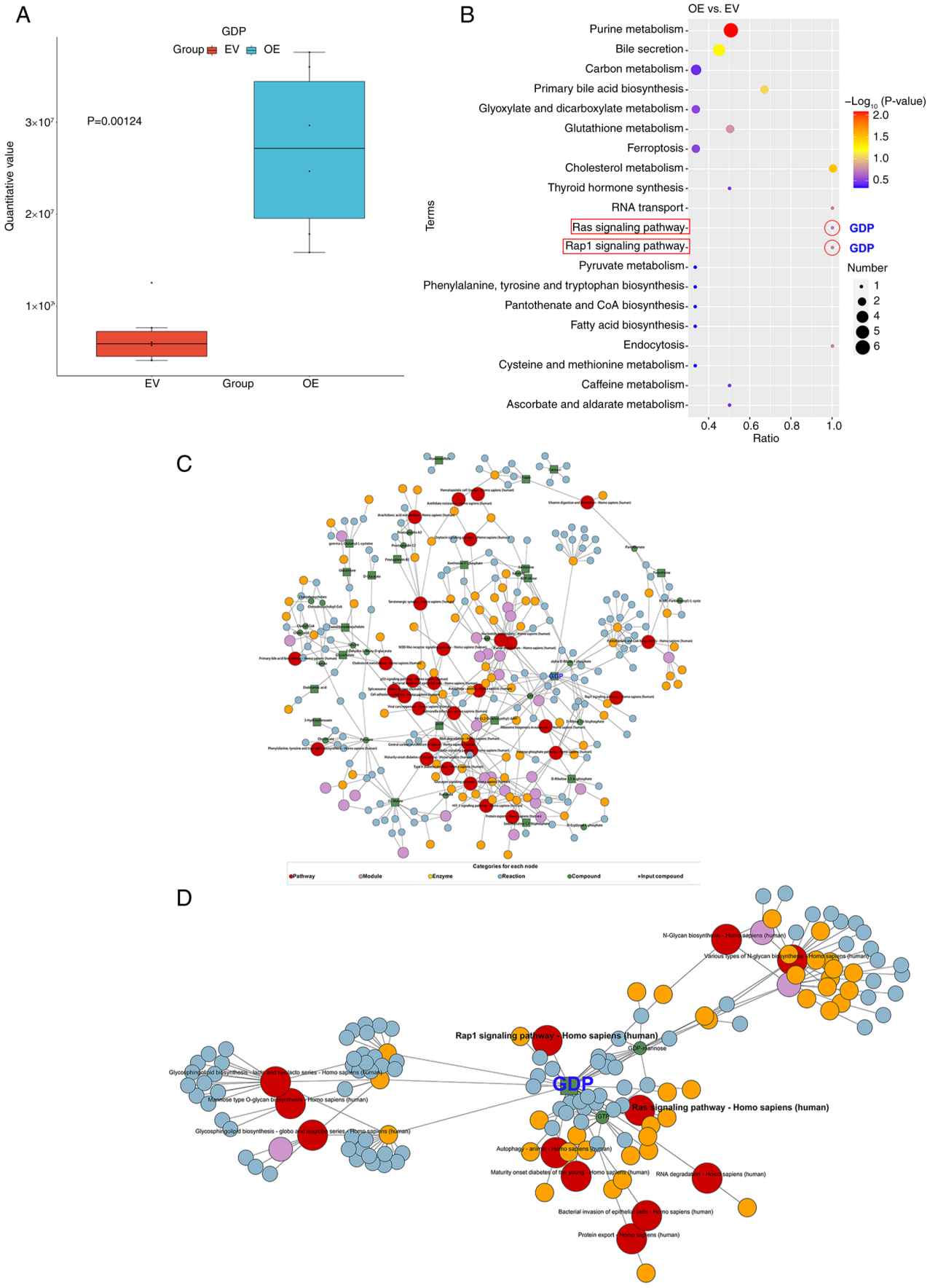

Figure 4. Differential metabolite abundance changes and network diagrams in HepG2 cells after FAXDC2 overexpression detected by untargeted metabolomics. (A) GDP expression in the FAXDC2 overexpression and control groups. (B) Bubble plot of KEGG pathway enrichment. The pathways enclosed in a red box are enriched only with GDP as a differential metabolite. (C) Overall KEGG regulatory network diagram and (D) reconstructed KEGG regulatory network diagram focusing on GDP. FAXDC2, fatty acid hydroxylase domain containing 2; GDP, guanosine diphosphate; OE, overexpression; EV, empty vector; KEGG, Kyoto Encyclopedia of Genes and Genomes.

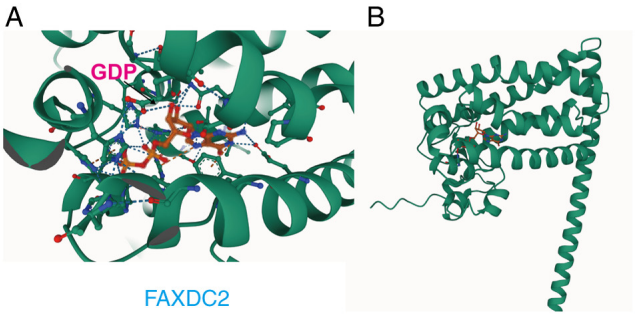

Figure 5. Structural prediction of the interaction between FAXDC2 and GDP performed by AlphaFold3. (A) Prediction of the binding site of FAXDC2 and GDP. (B) is the overall structure of (A). The dotted lines represent hydrogen bonds, the brown structure represents GDP, the blue spheres represent nitrogen atoms, and the red spheres represents oxygen atoms. FAXDC2, fatty acid hydroxylase domain containing 2; GDP, guanosine diphosphate.

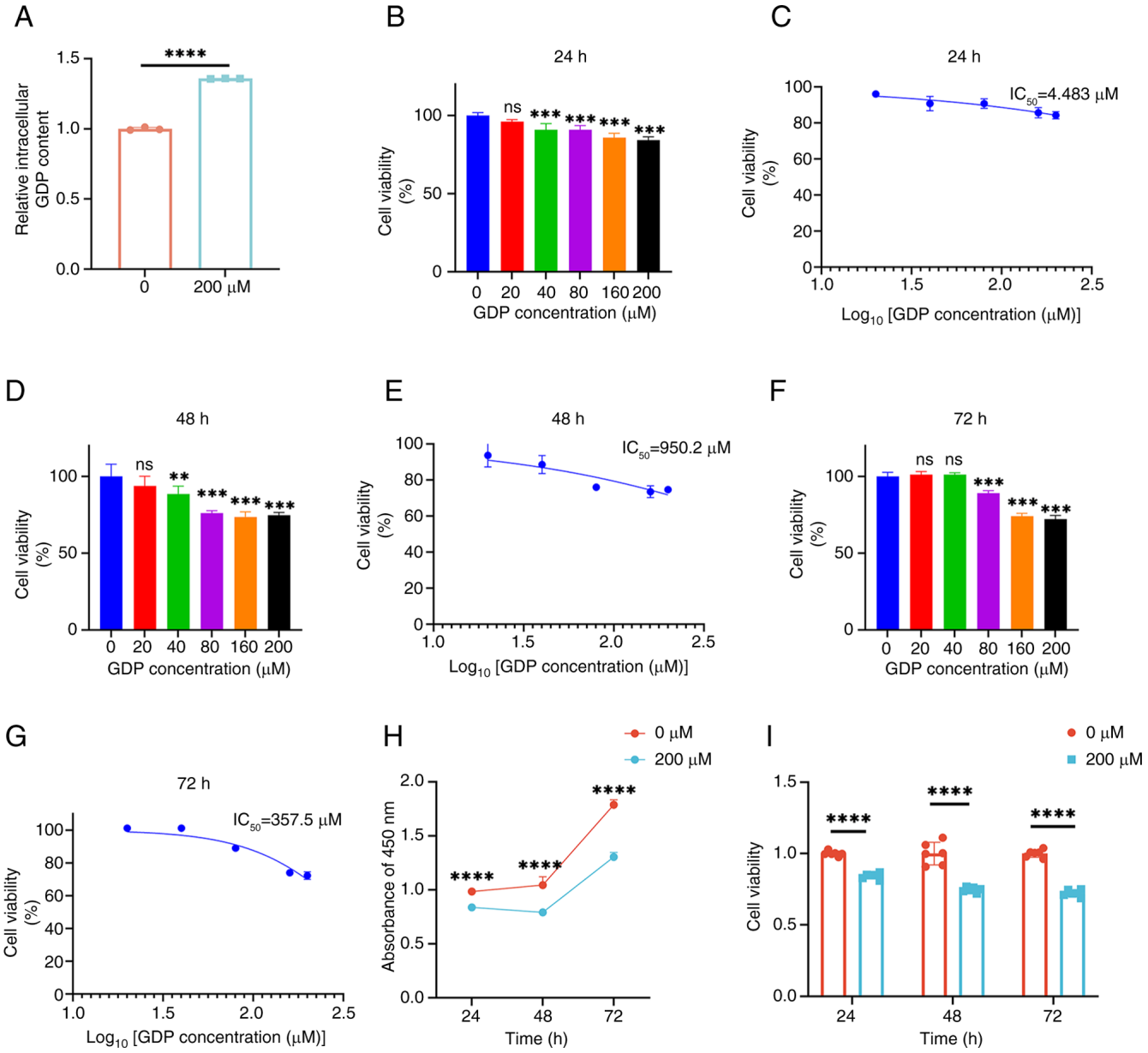

Figure 6. Changes in the proliferation activity of HepG2 cells after GDP treatment measured by Cell Counting Kit-8 assay. (A) Detection of the relative intracellular content of GDP in HepG2 cells by ELISA. (B) Viability of HepG2 cells 24 h after treatment with different concentrations of GDP and (C) the corresponding IC_{50}. (D) Viability of HepG2 cells 48 h after treatment with different concentrations of GDP and (E) the corresponding IC_{50}. (F) Viability of HepG2 cells 72 h after treatment with different concentrations of GDP and (G) the corresponding IC_{50}. (H) Changes in the absorbance at 450 nm of HepG2 cells treated with 200 μM GDP for 24, 48 and 72 h. (I) Comparison of the viability of HepG2 cells treated with 200 μM GDP for 24, 48 and 72 h. Each experimental group consisted of six biological replicates. GDP, guanosine diphosphate; IC_{50}, half-maximal inhibitory concentration; ns, not significant; **P<0.01, ***P<0.001, ****P<0.0001.

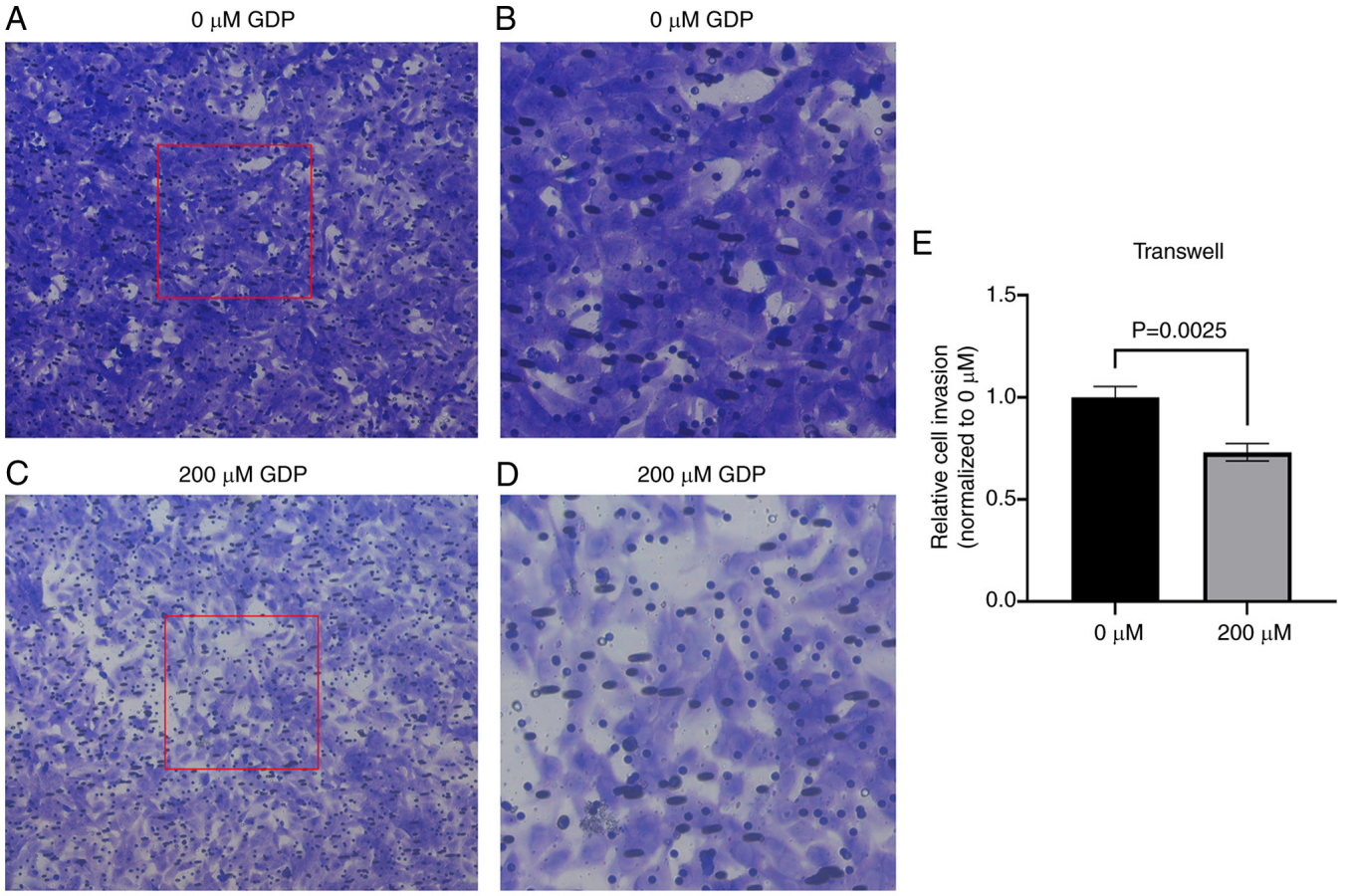

Figure 7. Assessment of the invasive ability of HepG2 cells after GDP treatment via Transwell assay. (A) Invasion results of untreated HepG2 cells (magnification, x100) and (B) magnified view of the red-boxed area in (A). (C) Invasion results of HepG2 cells treated with 200 μM GDP (magnification, x100) and (D) magnified view of the red-boxed area in (C). (E) Quantitative analysis of the invasion experiment. Each experimental group consisted of three biological replicates. GDP, guanosine diphosphate.

FAXDC2 interacts with GDP. Given the observation that the overexpression of FAXDC2 elicits alterations in the GDP content of HepG2 cells at the metabolic level, the advanced protein structure prediction tool, AlphaFold3 (28), was employed to model the three-dimensional structures of FAXDC2 and GDP (Fig. 5). This predicted a direct interaction between FAXDC2 and GDP, thereby suggesting a potential mechanistic link. Consequently, it was hypothesized that GDP may mediate the inhibitory effect of FAXDC2 on HepG2 cells, which may serve as a basis for understanding the molecular mechanisms underlying this process.

GDP inhibits HepG2 cell proliferation. Based on the findings of the metabolomics analysis and the absence of direct reports on the inhibitory effects of GDP on tumors in previous studies, the present study aimed to directly validate the effects of GDP on the HepG2 cell line. The GDP concentrations used were selected with reference to those used in the study by Traut (32). Initially, ELISA experiments were conducted to detect the GDP content of HepG2 cells following treatment with 200 μM GDP (Fig. 6A). It was observed that the intracellular GDP content increased by ~35% after treatment with 200 μM GDP compared with that in cells without GDP treatment.

The proliferation of HepG2 cells was then evaluated using the CCK-8 assay. The results indicated that a significant reduction in the viability of HepG2 cells occurred following treatment with 40-200 μM GDP compared with that in the control group (Fig. 6). Moreover, the inhibitory effect of GDP gradually intensified as its concentration increased, suggesting a concentration-dependent effect of GDP on the inhibition of HepG2 cell activity. Additionally, as shown in Fig. 6B-G, the inhibitory effect of GDP on HepG2 cells increased over time, compared with that in the control group. Specifically, following GDP treatment, the IC_{50} values decreased from 4,483 μM at 24 h to 950.2 μM at 48 h, and further to 357.5 μM at 72 h.

A 200 μM concentration of GDP was selected for use in subsequent experiments. The viability of HepG2 cells treated with 200 μM GDP for 24, 48 and 72 h was measured, as shown in Fig. 6H and I. The viability of HepG2 cells was significantly decreased after treatment with 200 μM GDP at each time point. These results indicate that GDP inhibits the proliferation of HepG2 cells.

GDP inhibits HepG2 cell invasion. To comprehensively evaluate the inhibitory effects of GDP on liver cancer, a Transwell assay was performed to assess the invasive ability of HepG2 cells after treatment with 200 μM GDP (Fig. 7). The number of HepG2 cells passing through the Transwell membrane significantly decreased following treatment with 200 μM GDP

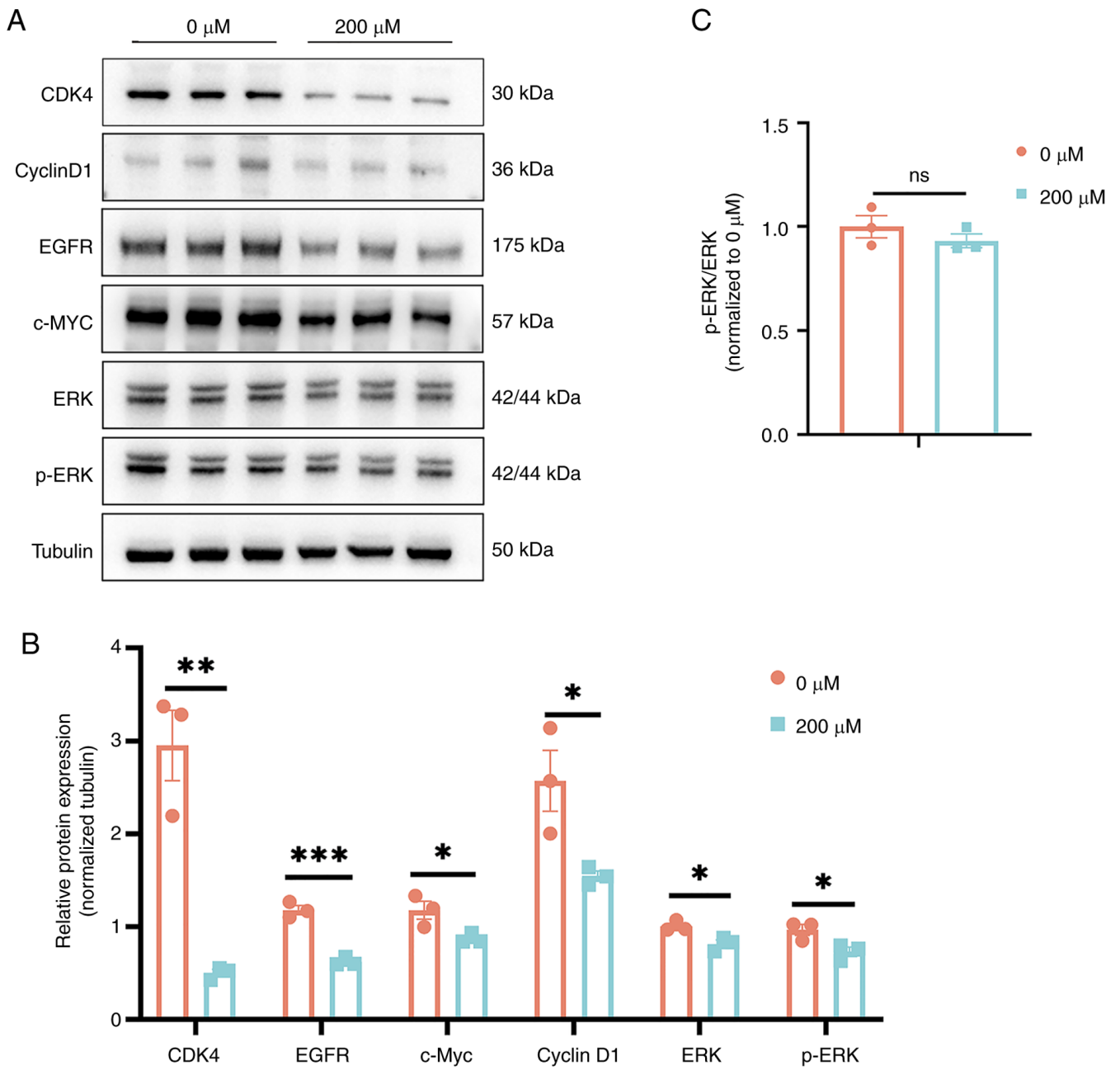

Figure 8. Evaluation of ERK signal transduction in HepG2 cells following treatment with GDP. (A) Impact of GDP treatment on proliferation-related proteins and ERK activity shown in representative western blots. (B) Quantitative analysis of the western blotting data (n=3). (C) pERK/ERK ratio. *P<0.05, **P<0.01 and ***P<0.001. GDP, guanosine diphosphate; CDK4, cyclin-dependent kinase 4; EGFR, epidermal growth factor receptor; ERK, extracellular signal-regulated kinase; p-ERK, phosphorylated ERK; ns, not significant.

compared with that of untreated cells, indicating a significant inhibition of the invasive ability of HepG2 cells by GDP.

GDP inhibits MAPK/ERK signaling. To explore the impact of increased GDP levels on the signaling pathways within HepG2 cells, guided by metabolomic insights, key signaling molecules in the Ras/ERK pathway and several proteins associated with cell proliferation were examined via western blot analysis (Fig. 8). The results demonstrated that after the treatment of HepG2 cells with 200 μM GDP, the expression levels of ERK, EGFR, c-Myc and the cell cycle-related proteins, CDK4 and cyclin D1, were all significantly downregulated. These findings suggest that an increase in GDP levels may inhibit the Ras/ERK signaling pathway.

Discussion

Lipid metabolism is closely associated with the occurrence and development of liver cancer (33). Our previous study indicated that FAXDC2 is significantly downregulated in various types of cancer tissues, including liver cancer, and its low expression is closely associated with a poor prognosis in patients (23). Based on preliminary research findings, combined with the metabolomics and experimental biology analyses performed in the present study, it is proposed that: i) FAXDC2 inhibits

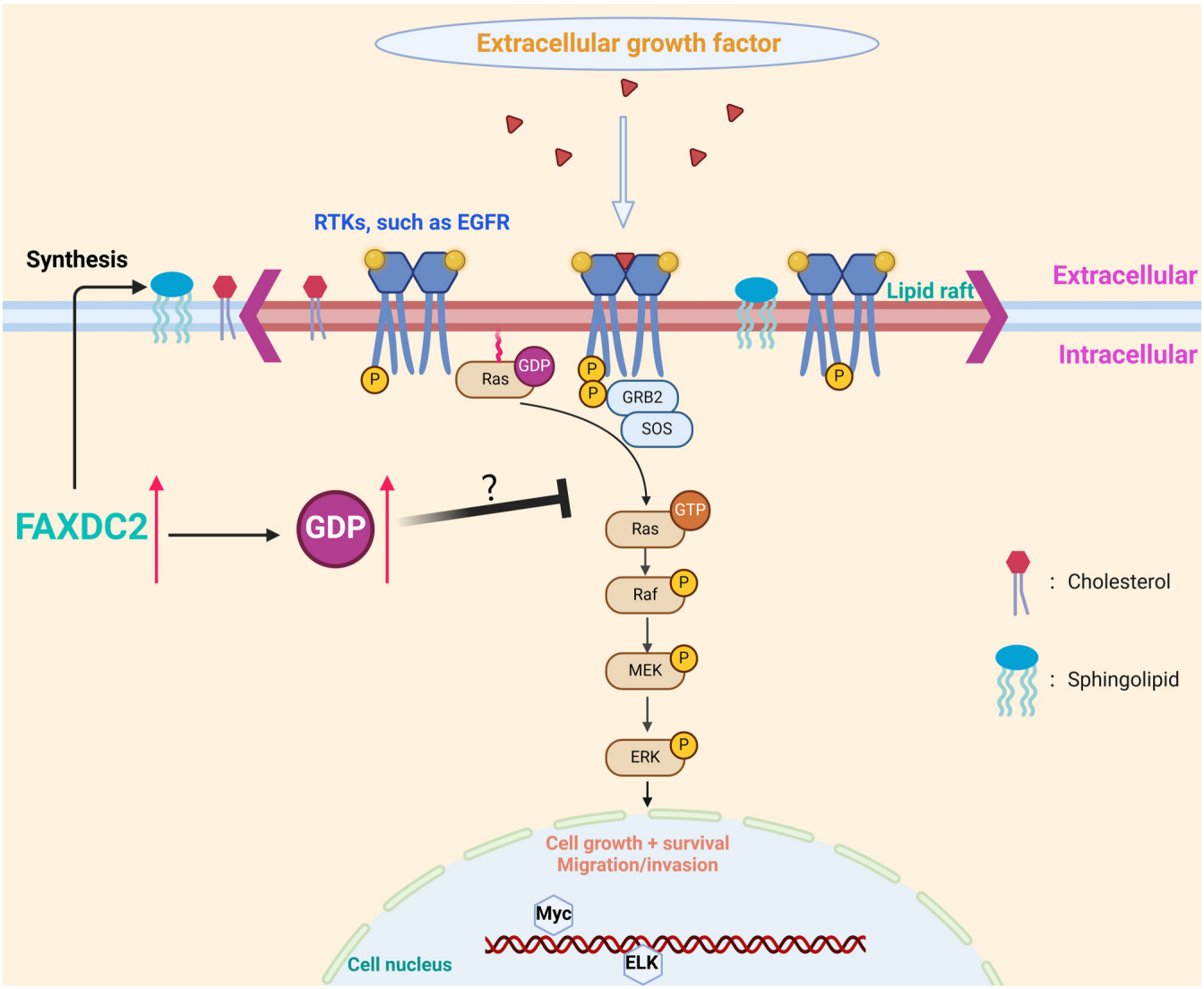

Figure 9. Diagram of the potential role of GDP in HepG2 cells. It is speculated that GDP competes with GTP for binding to Ras, leaving Ras in an inactivated state, thereby inhibiting downstream gene transduction. GDP, guanosine diphosphate; GTP, guanosine triphosphate; FAXCD2, fatty acid hydroxylase domain containing 2; RTKs, receptor tyrosine kinases; EGFR, epidermal growth factor receptor; GRB2, growth factor receptor-bound protein 2; SOS, son of seven-less; ERK, extracellular signal-regulated kinase; ELK, Ets-like; p, phosphorylation.

the progression of liver cancer by modulating GDP concentration; and ii) GDP regulates HepG2 cell proliferation and invasion via the MAPK/ERK pathway.

The present study identified GDP as a significantly upregulated differential metabolite through metabolomics analysis following FAXDC2 overexpression. GDP had the highest VIP value among all differential metabolites, indicating that it made the greatest contribution to the differences between the experimental and control groups. Additionally, among the differentially enriched metabolites in the KEGG pathways, GDP was the only differential metabolite enriched in both the 'Ras signaling pathway' and 'Rap1 signaling pathway'. Therefore, the present study further investigated the impact of an elevated GDP concentration on the Ras/ERK signaling pathway. Through western blot analysis, it was observed that the increase in GDP content significantly inhibited ERK expression. A potential explanation of the process by which elevated intracellular concentrations of GDP induce changes in Ras activity is protein succinylation, a modification that can be influenced by the concentration of succinyl-CoA within mitochondria (34). There may be a discrete subcellular compartment where Ras activity is regulated by GDP concentration, operating independently of the canonical mechanism involving GTPase-activating protein (GAP) and guanine nucleotide exchange factors. However, this hypothesis requires rigorous empirical validation through ongoing and future investigations.

A common hallmark of tumor growth signaling mediated by the Ras/Raf/MEK/ERK cascade within the MAPK/ERK pathway is the sustained activation of ERK1/2 (35). Ras and Raf are known to be oncogenes, and Ras/Raf/MEK/ERK signaling is activated in ~50% of patients with early-stage liver cancer and nearly all patients with late-stage liver cancer (36). In addition, it has been shown that specific inhibition of MEK1 blocks ERK1/2 phosphorylation, and dose-dependently inhibits the proliferation of liver cancer cells (37). The Ras isoforms H-Ras, K-Ras and N-Ras regulate cell proliferation, survival and differentiation (38), by acting as a critical component in numerous signal transduction

processes and functioning as a 'switch'. When activated, the Raf serine/threonine kinases are recruited to the plasma membrane, triggering the activation of the ERK signaling pathway and other targets (39). In the active GTP-bound state, Ras proteins undergo conformational changes, which allow them to bind to effector proteins and contribute to signal transduction (40). Intrinsic Ras GTPases convert Ras-GTP to Ras-GDP by hydrolysis with the assistance of GAPs; this renders Ras inactive and stops signal transduction (40).

A number of studies have shown that GDP, as a metabolite of GTP, competes with GTP for binding to the small G protein Ras, thereby facilitating the interconversion of Ras between its active (Ras-GTP) and inactive (Ras-GDP) states (41-43). In its inactive state, Ras/Raf/ERK signal transduction is blocked, which leads to a reduction in cell proliferation capacity. Studies have shown that even when GPCRs are not catalytically active, tumors can be promoted by the acceleration of GDP dissociation from the receptors (44-46). Despite this, few studies have reported on the role of GDP in cancer cells.

A comprehensive investigation conducted by Traut (32) in 1994 meticulously elucidated the distribution patterns of GDP in diverse human cellular populations, encompassing lymphocytes, monocytes, neutrophils, platelets, eosinophils and erythrocytes, in addition to its presence in rat liver tissue and hepatocellular carcinoma. Leveraging their findings as a foundation, the application of a range of GDP concentrations to HepG2 cells was performed in the present study, with the subsequent analysis of cell viability by CCK-8 assay. The analysis revealed that 200 μM GDP had a pronounced inhibitory effect on HepG2 cells. Consequently, a 200 μM GDP concentration was selected as the treatment standard for HepG2 cells in the present study. Overall, the results of the present study indicate that overexpression of FAXDC2 leads to an increase in GDP levels, which may inhibit Ras activity, thereby suppressing Ras/Raf/ERK signal transduction (Fig. 9). This was confirmed by western blotting results, which are consistent with those in our previous study, which concluded that FAXDC2 inhibits ERK phosphorylation, thereby suppressing the occurrence and development of liver cancer (23). AlphaFold3 predicted a potential direct interaction between FAXDC2 and GDP, thus indicating the importance of investigating whether increased GDP concentrations influence the enzymatic activity of FAXDC2. Concerning the mechanism by which FAXDC2 potentially regulates GDP levels, the non-targeted metabolomics profiling revealed insignificant or undetectable changes in the levels of GDP-related metabolites, such as guanosine monophosphate, guanosine triphosphate, deoxy-GDP and guanosine tetraphosphate. Therefore, it is speculated that FAXDC2 adjusts intracellular GDP levels via an obscure and as yet uncharacterized pathway. To comprehensively determine the specific mechanisms of this pathway, an in-depth investigation will be performed in a future study with the aim of uncovering the underlying principles.

The direct treatment of HepG2 cells with GDP was observed to inhibit the proliferation and invasion of the cells, as determined by CCK-8, Transwell and western blotting assays. The results also suggest that GDP inhibits cancer cell growth in a concentration-dependent manner. The direct inhibition of small molecules has great potential in the treatment of diseases. Research has shown that the administration of nicotinamide mononucleotide (NMN), which can directly regulate disease, for up to 12 months can effectively combat aging without significant toxicity, severe side effects or increased mortality rates, indicating its long-term safety (47). Similarly, another study demonstrated that NMN has anti-aging effects on mice (48). In addition, the metabolically active small molecule resveratrol can be directly used to prevent a variety of diseases, including obesity (49), aging (50,51) and neurodegenerative diseases (52). Notably, a previous study demonstrated that an intraperitoneal injection of resveratrol ameliorated the oxidative stress-induced aging damage of oocytes after ovulation in middle-aged mice (53). However, there are few reports on the direct inhibition of liver cancer via the metabolism of small molecule substances. As a metabolite involved in tumor metabolic reprogramming, GDP is likely to play an inhibitory role in the process of tumor occurrence and development. Moreover, as it is a substance produced metabolically in the body, GDP is unlikely to cause harm during its anticancer action. Furthermore, in the present investigation of the GDP content of HepG2 cells, it was noted that the intracellular GDP concentration in HepG2 cells treated with 200 μM GDP increased by only 35% compared with that in the untreated control group. This finding suggests that GDP might not only enter cells to perform its functions but could also interact with receptors on the cell membrane to exert its effects. This suggestion warrants further exploration and elucidation in subsequent studies.

It is imperative to acknowledge that, despite the innovative nature of the present study, it is not without limitations. Notably, it did not directly demonstrate that GDP mediates the inhibitory effects of FAXDC2 on HepG2 cells. Moreover, exploration of the underlying mechanisms remains relatively superficial, necessitating a more detailed investigation in subsequent studies. Furthermore, given that the HepG2 cell line originates from hepatoblastoma, it is not typically considered a representative model of a hepatocellular carcinoma cell line. Therefore, the scope of the validation process will be broadened to encompass a greater diversity of liver cancer cells in future studies, with the objective of deriving more detailed conclusions. In addition, the effects of GDP were only examined in cells, and no *in vivo* experiments were performed using animals to further evaluate its function within a biological context. In addition, whether there is any difference in intracellular GDP concentration in humans between physiological conditions and cancerous states was not detected. In follow-up studies, the difference in GDP concentration between cancer tissues and adjacent tissues in liver cancer patients will be analyzed, to more accurately evaluate the potential of GDP as a small molecule inhibitor. These limitations will serve as pivotal targets for future studies.

In summary, to the best of our knowledge, the present study is the first to demonstrate that GDP can directly inhibit the proliferation and invasion of HepG2 cells. This study provides experimental evidence that may be relevant to the development of liver cancer and may aid in the search for new diagnostic and intervention methods.

Acknowledgements

Not applicable.

Funding

This study was supported in part by grants from the National Natural Science Foundation of China (grant nos. 81970324 and 81974019), Shanghai Key Laboratory of Regulatory Biology, Institute of Biomedical Sciences, East China Normal University, National Key Research and Development Program of China (grant no. 2018YFA0108700), Guangzhou Science and Technology Plan Project (grant no. 202201000006) and Guangdong Provincial Special Support Program for Prominent Talents (grant no. 2021JC06Y656).

Availability of data and materials

The data generated in the present study may be requested from the corresponding author. The metabolomics data generated in the present study may be found in the National Omics Data Encyclopedia (NODE) under accession number OEP00005871 or at the following URL: https://www.biosino.org/node/browse?keyword=OEP00005871.

Authors' contributions

Conceptualization was performed by ZP, WY, YW and XF. Methodology was the responsibility of XW and FL. Data analysis was performed by SX, PZ, YL and HW. Data validation was performed by ZhoJ, SL and YH. Formal analysis was conducted by ZP, ML, ZhiJ, YC and YS. Research background investigations (including researching the experimental scheme) were carried out by ZP and ML. Resources were obtained by FL, YW and YS. Data was curated by ZhiJ, YS and YC. The original draft of the manuscript was prepared by ZP, and reviewed and edited by XF, PZ, YL and XW. Language editing was performed by PZ, YL, ZhiJ, ML and FL. Data visualization (for mapping and typesetting the obtained data) was performed by YW, YC and WY. Supervision was by YL, HW and FL, project administration was by WY, SX, HW and FL, and funding was acquired by XF and PZ. ZP and XF confirm the authenticity of all the raw data. All authors read and approved the final version of the manuscript.

Ethics approval and consent to participate

Not applicable.

Patient consent for publication

Not applicable.

Competing interests

The authors declare that they have no competing interests.

References

1. Siegel RL, Miller KD, Wagle NS and Jemal A: Cancer statistics, 2023. CA Cancer J Clin 73: 17-48, 2023.
2. Gao S, Gang J, Yu M, Xin G and Tan H: Computational analysis for identification of early diagnostic biomarkers and prognostic biomarkers of liver cancer based on GEO and TCGA databases and studies on pathways and biological functions affecting the survival time of liver cancer. BMC cancer 21: 791, 2021.
3. Yang WS, Zeng XF, Liu ZN, Zhao QH, Tan YT, Gao J, Li HL and Xiang YB: Diet and liver cancer risk: A narrative review of epidemiological evidence. Br J Nutr 124: 330-340, 2020.
4. Anwanwan D, Singh SK, Singh S, Saikam V and Singh R: Challenges in liver cancer and possible treatment approaches. Biochim Biophys Acta Rev Cancer 1873: 188314, 2020.
5. Li S, Yin S, Ding H, Shao Y, Zhou S, Pu W, Han L, Wang T and Yu H: Polyphenols as potential metabolism mechanisms regulators in liver protection and liver cancer prevention. Cell Prolif 56: e13346, 2023.
6. Raoul JL, Forner A, Bolondi L, Cheung TT, Kloeckner R and de Baere T: Updated use of TACE for hepatocellular carcinoma treatment: How and when to use it based on clinical evidence. Cancer Treat Rev 72: 28-36, 2019.
7. Llovet JM, Kelley RK, Villanueva A, Singal AG, Pikarsky E, Roayaie S, Lencioni R, Koike K, Zucman-Rossi J and Finn RS: Hepatocellular carcinoma. Nat Rev Dis Primers 7: 6, 2021.
8. Luo X, Cheng C, Tan Z, Li N, Tang M, Yang L and Cao Y: Emerging roles of lipid metabolism in cancer metastasis. Mol Cancer 16: 76, 2017.
9. Yi M, Li J, Chen S, Cai J, Ban Y, Peng Q, Zhou Y, Zeng Z, Peng S, Li X, *et al*: Emerging role of lipid metabolism alterations in cancer stem cells. J Exp Clin Cancer Res 37: 118, 2018.
10. Medes G, Thomas A and Weinhouse S: Metabolism of neoplastic tissue. IV. A study of lipid synthesis in neoplastic tissue slices in vitro. Cancer Res 13: 27-29, 1953.
11. Ookhtens M, Kannan R, Lyon I and Baker N: Liver and adipose tissue contributions to newly formed fatty acids in an ascites tumor. Am J Physiol 247: R146-R153, 1984.
12. Yang H, Deng Q, Ni T, Liu Y, Lu L, Dai H, Wang H and Yang W: Targeted Inhibition of LPL/FABP4/CPT1 fatty acid metabolic axis can effectively prevent the progression of nonalcoholic steatohepatitis to liver cancer. Int J Biol Sci 17: 4207-4222, 2021.
13. Wu D, Yang Y, Hou Y, Zhao Z, Liang N, Yuan P, Yang T, Xing J and Li J: Increased mitochondrial fission drives the reprogramming of fatty acid metabolism in hepatocellular carcinoma cells through suppression of Sirtuin 1. Cancer Commun (Lond) 42: 37-55, 2022.
14. Wang W, Bai L, Li W and Cui J: The lipid metabolic landscape of cancers and new therapeutic perspectives. Front Oncol 10: 605154, 2020.
15. Beloribi-Djefaflia S, Vasseur S and Guillaumond F: Lipid metabolic reprogramming in cancer cells. Oncogenesis 5: e189, 2016.
16. Du D, Liu C, Qin M, Zhang X, Xi T, Yuan S, Hao H and Xiong J: Metabolic dysregulation and emerging therapeutical targets for hepatocellular carcinoma. Acta Pharm Sin B 12: 558-580, 2022.
17. Sun Y, Liu WZ, Liu T, Feng X, Yang N and Zhou HF: Signaling pathway of MAPK/ERK in cell proliferation, differentiation, migration, senescence and apoptosis. J Recept Signal Transduct Res 35: 600-604, 2015.
18. Delire B and Stärkel P: The Ras/MAPK pathway and hepatocarcinoma: Pathogenesis and therapeutic implications. Eur J Clin Invest 45: 609-623, 2015.
19. Dimri M and Satyanarayana A: Molecular signaling pathways and therapeutic targets in hepatocellular carcinoma. Cancers (Basel) 12: 491, 2020.
20. Peng Y, Song Y and Wang H: Systematic elucidation of the aneuploidy landscape and identification of aneuploidy driver genes in prostate cancer. Front Cell Dev Biol 9: 723466, 2021.
21. Zhang P, Ma K, Ke X, Liu L, Li Y, Liu Y and Wang Y: Development and validation of a Five-RNA-Based signature and identification of candidate drugs for neuroblastoma. Front Genet 12: 685646, 2021.
22. Jin Q, Ren Y, Wang M, Suraneni PK, Li D, Crispino JD, Fan J and Huang Z: Novel function of FAXDC2 in megakaryopoiesis. Blood Cancer J 6: e478, 2016.
23. Peng Z, Xu S, Zhang Q, Yang X, Yuan W, Wang Y, Li Y, Zhu P, Wu X, Jiang Z, *et al*: FAXDC2 inhibits the proliferation and invasion of human liver cancer HepG2 cells. Exp Ther Med 27: 27, 2024.
24. Livak KJ and Schmittgen TD: Analysis of relative gene expression data using real-time quantitative PCR and the 2(-Delta Delta C(T)) method. Methods 25: 402-408, 2001.
25. Rao G, Sui J and Zhang J: Metabolomics reveals significant variations in metabolites and correlations regarding the maturation of walnuts (Juglans regia L.). Biol Open 5: 829-836, 2016.
26. Boulesteix AL and Strimmer K: Partial least squares: A versatile tool for the analysis of high-dimensional genomic data. Brief Bioinform 8: 32-44, 2007.

27. Wen B, Mei Z, Zeng C and Liu S: metaX: A flexible and comprehensive software for processing metabolomics data. BMC Bioinformatics 18: 183, 2017.
28. Abramson J, Adler J, Dunger J, Evans R, Green T, Pritzel A, Ronneberger O, Willmore L, Ballard AJ, Bambrick J, *et al*: Accurate structure prediction of biomolecular interactions with AlphaFold 3. Nature 630: 493-500, 2024.
29. Wu M, Zhao Y, Tao M, Fu M, Wang Y, Liu Q, Lu Z and Guo J: Malate-based biodegradable scaffolds activate cellular energetic metabolism for accelerated wound healing. ACS Appl Mater Interfaces 15: 50836-50853, 2023.
30. Adeva-Andany MM, Pérez-Felpete N, Fernández-Fernández C, Donapetry-García C and Pazos-García C: Liver glucose metabolism in humans. Biosci Rep 36: e00416, 2016.
31. Vetter IR and Wittinghofer A: The guanine nucleotide-binding switch in three dimensions. Science 294: 1299-1304, 2001.
32. Traut TW: Physiological concentrations of purines and pyrimidines. Mol Cell Biochem 140: 1-22, 1994.
33. Ni T, He Z, Dai Y, Yao J, Guo Q and Wei L: Oroxylin A suppresses the development and growth of colorectal cancer through reprogram of HIF1α-modulated fatty acid metabolism. Cell Death Dis 8: e2865, 2017.
34. Ali HR, Michel CR, Lin YH, McKinsey TA, Jeong MY, Ambardekar AV, Cleveland JC, Reisdorph R, Reisdorph N, Woulfe KC and Fritz KS: Defining decreased protein succinylation of failing human cardiac myofibrils in ischemic cardiomyopathy. J Mol Cell Cardiol 138: 304-317, 2020.
35. Cook SJ, Stuart K, Gilley R and Sale MJ: Control of cell death and mitochondrial fission by ERK1/2 MAP kinase signalling. FEBS J 284: 4177-4195, 2017.
36. Llovet JM, Villanueva A, Lachenmayer A and Finn RS: Advances in targeted therapies for hepatocellular carcinoma in the genomic era. Nat Rev Clin Oncol 12: 408-424, 2015.
37. Wiesenauer CA, Yip-Schneider MT, Wang Y and Schmidt CM: Multiple anticancer effects of blocking MEK-ERK signaling in hepatocellular carcinoma. J Am Coll Surg 198: 410-421, 2004.
38. Yang J, Pan WH, Clawson GA and Richmond A: Systemic targeting inhibitor of kappaB kinase inhibits melanoma tumor growth. Cancer Res 67: 3127-3134, 2007.
39. Roy S, Luetterforst R, Harding A, Apolloni A, Etheridge M, Stang E, Rolls B, Hancock JF and Parton RG: Dominant-negative caveolin inhibits H-Ras function by disrupting cholesterol-rich plasma membrane domains. Nat Cell Biol 1: 98-105, 1999.
40. Higgins EM, Bos JM, Mason-Suares H, Tester DJ, Ackerman JP, MacRae CA, Sol-Church K, Gripp KW, Urrutia R and Ackerman MJ: Elucidation of MRAS-mediated Noonan syndrome with cardiac hypertrophy. JCI Insight 2: e91225, 2017.
41. Xu J, Hedberg C, Dekker FJ, Li Q, Haigis KM, Hwang E, Waldmann H and Shannon K: Inhibiting the palmitoylation/depalmitoylation cycle selectively reduces the growth of hematopoietic cells expressing oncogenic Nras. Blood 119: 1032-1035, 2012.
42. Wang Y, Ji D, Lei C, Chen Y, Qiu Y, Li X, Li M, Ni D, Pu J, Zhang J, *et al*: Mechanistic insights into the effect of phosphorylation on Ras conformational dynamics and its interactions with cell signaling proteins. Comput Struct Biotechnol J 19: 1184-1199, 2021.
43. Li Q, Haigis KM, McDaniel A, Harding-Theobald E, Kogan SC, Akagi K, Wong JC, Braun BS, Wolff L, Jacks T and Shannon K: Hematopoiesis and leukemogenesis in mice expressing oncogenic NrasG12D from the endogenous locus. Blood 117: 2022-2032, 2011.
44. Kan Z, Jaiswal BS, Stinson J, Janakiraman V, Bhatt D, Stern HM, Yue P, Haverty PM, Bourgon R, Zheng J, *et al*: Diverse somatic mutation patterns and pathway alterations in human cancers. Nature 466: 869-873, 2010.
45. Garcia-Marcos M, Ghosh P and Farquhar MG: Molecular basis of a novel oncogenic mutation in GNAO1. Oncogene 30: 2691-2696, 2011.
46. Leyme A, Marivin A, Casler J, Nguyen LT and Garcia-Marcos M: Different biochemical properties explain why two equivalent Gα subunit mutants cause unrelated diseases. J Biol Chem 289: 21818-21827, 2014.
47. Mills KF, Yoshida S, Stein LR, Grozio A, Kubota S, Sasaki Y, Redpath P, Migaud ME, Apte RS, Uchida K, *et al*: Long-term administration of nicotinamide mononucleotide mitigates Age-associated physiological decline in mice. Cell Metab 24: 795-806, 2016.
48. de Picciotto NE, Gano LB, Johnson LC, Martens CR, Sindler AL, Mills KF, Imai S and Seals DR: Nicotinamide mononucleotide supplementation reverses vascular dysfunction and oxidative stress with aging in mice. Aging Cell 15: 522-530, 2016.
49. Wang S, Liang X, Yang Q, Fu X, Zhu M, Rodgers BD, Jiang Q, Dodson MV and Du M: Resveratrol enhances brown adipocyte formation and function by activating AMP-activated protein kinase (AMPK) α1 in mice fed high-fat diet. Mol Nutr Food Res 61: 10, 2017 .
50. Pearson KJ, Baur JA, Lewis KN, Peshkin L, Price NL, Labinskyy N, Swindell WR, Kamara D, Minor RK, Perez E, *et al*: Resveratrol delays age-related deterioration and mimics transcriptional aspects of dietary restriction without extending life span. Cell Metab 8: 157-168, 2008.
51. Park SJ, Ahmad F, Philp A, Baar K, Williams T, Luo H, Ke H, Rehmann H, Taussig R, Brown AL, *et al*: Resveratrol ameliorates aging-related metabolic phenotypes by inhibiting cAMP phosphodiesterases. Cell 148: 421-433, 2012.
52. Bernier M, Wahl D, Ali A, Allard J, Faulkner S, Wnorowski A, Sanghvi M, Moaddel R, Alfaras I, Mattison JA, *et al*: Resveratrol supplementation confers neuroprotection in cortical brain tissue of nonhuman primates fed a high-fat/sucrose diet. Aging (Albany NY) 8: 899-916, 2016.
53. Liang QX, Lin YH, Zhang CH, Sun HM, Zhou L, Schatten H, Sun QY and Qian WP: Resveratrol increases resistance of mouse oocytes to postovulatory aging in vivo. Aging (Albany NY) 10: 1586-1596, 2018.